2021 IEEE International Joint Conference on Biometrics (IJCB) | 978-1-6654-3780-6/21/$31.00 ©2021 IEEE | DOI: 10.1109/IJCB52358.2021.9484364

Optimizing contactless to contact-based fingerprint comparison using simple parametric warping models

Dominik Söllinger and Andreas Uhl
Multimedia Signal Processing and Security Lab
University of Salzburg
5020 Salzburg, Austria
dsoellinger@cs.sbg.ac.at

Abstract

2D contactless to contact-based fingerprint (FP) comparison is a challenging task due to different types of distortion introduced during the capturing process. While contact-based FPs typically exhibit a wide range of elastic distortions, perspective distortions pose a problem in contactless FP imagery. In this work, we investigate three simple parametric warping models for contactless fingerprints — circular, elliptical and bidirectional warping — and show that these models can be used to improve the interoperability between the two modalities by simulating unfolding of a generic 3D model. Additionally, we employ score fusion as a technique to enhance the comparison performance in scenarios where multiple contactless FPs of the same finger are available. Using the simple circular warping, we have been able to decrease the Equal Error Rate (EER) from 1.79% to 0.78% and 1.82% to 1.31% on our dataset, respectively.

1. Introduction

During the last decade, many solutions for contactless FP recognition have been developed [7]. These solutions offer many advantages over traditional contact-based solutions such as better hygiene and better user acceptance due to the less constrainted capturing environment. However, the fact that FPs have been acquired in a contact-based manner for decades raises the question if an "old" contact-based FP can be compared with a "new" contactless FP.

From several publications [11, 12, 14] we know that the FP comparison performance drops dramatically when comparison FPs captured with different sensors, especially when the fingerprints are captured with contactless and contact-based sensors [2, 15, 9, 5, 8]. An obvious reason that negatively impacts the sensor interoperability of contact-based and contactless FPs, is in the nature of contact-based FP acquisition where a finger is pressed or rolled against a platten surface. Pressing/Rolling inevitably leads to elastic distortions. On the other hand, contactless FP sensors have a higher risk of being negatively impacted by perspective distortions due to the high degree of freedom available to fingers along the three axes during the sensing.

Various publications directly address the problem of the elastic distortions in the context of 2D contactless to contact-based FP comparison. Lin and Kumar [10] proposed a generalized deformation correction model which relies on robust thin-plate splines. The authors concluded that the current cross-comparison error rates are not yet low enough for deployment but perspective distortion correction is expected to reduce the error rates.

Dabouei *et al*. [3] proposed the use of a TPS (Thin Plate Spline) model with warping parameters directly learned by a neural network. Their method also implicitly provides a way to transfer the style of contact-based FP images to contactless images. We ourselves we found their approach to have problems if contact-based FP impressions as groundtruth for training exhibit strongly varying deformations, rotations and positions.

A solution to this problem was recently presented in [6]. Instead of directly using contact-based FPs as groundtruth for TPS parameter prediction, textural representations from 2D contact-based and 2D contactless FPs extracted using a CNN (DeepPrint [4]) were used as groundtruth. Unfortunately, the approach also requires a (pre-)trained DeepPrint model.

Not directly concerned with contact-based to contactless FP comparison but concerned with the problem of comparing multiple contactless FPs is [13]. The authors presented a CNN-based core point detection and pose-compensation approach in order to address unwanted pose changes with contactless FP samples. In their work the authors made use of an ellipsoidal model to approximate the shape of the finger.

1.1. Our work

Our work deals with the problem of 2D contactless to contact-based FP comparison. Recent work [13] showed that a simple parametric ellipsoidal model can be used to compensate the finger pose in contactless FP imagery by projecting the finger onto an ellipsoid and rotating the ellipsoid in 3D space. This raises the question if the approach can be extended to work for contactless to contact-based FP comparison by unfolding the 3D model onto a 2D plane. To answer this question we propose three different warping methods (circular, elliptical and bidirectional) which are based on three different parametric 3D models. We then test their ability to mimic the physical deformation of a finger that is pressed against a platen surface by investigating whether the contactless to contact-based FP comparison performance is improved. Additionally, we test max/mean score fusion as a technique to improve the comparison performance for scenarios where multiple contactless images are available. All experiments are conducted on a challenging, self-acquired dataset of contactless and contact-based FP images. All contactless FP images were captured with an standard iPhone without imposing restrictions on the hand placement or camera placement. Only the distance to the camera was implicitly constrainted by the use of a fixed focal length lens setting.

The paper is organized as follows: In Sec. 2 we present the three different warping methods/models which are investigated in this work. In Sec. 3 we detail the experimental setup. We introduce the dataset, explain the FP comparison pipeline and score fusion. In Sec 4 we report and discuss the results and in Sec. 5 we provide some concluding remarks.

2. Contactless fingerprints warping based on simple parametric 3D models

Contact-based fingerprints are typically captured by pressing or rolling of the finger against a platen surface. The result is a physical deformation of the skin due to the rolling motion. To be able to compare a contact-less fingerprint with a conventional contact-based fingerprint we need to simulate the physical deformation caused by the rolling motion by means of warping of the contactless fingerprint. Generally, this boils down to unfolding a 3D object (i.e., a 3D fingertip) onto a flat 2D plane. However, reconstructing the exact 3D shape of a finger from a set of contactless fingerprint is an extremely challenging tasks and it is almost impossible if we are only given a single fingerprint image. To overcome this problem in this work, we approximate the 3D finger shape using a simple parametric model for the finger such as a cylinder. Given a front-view image of the finger, we obtain the unwarped fingerprint by projecting the fingerprint texture onto the 3D-parametric model and unfolding the parametric model by simulating a rotation in various directions.

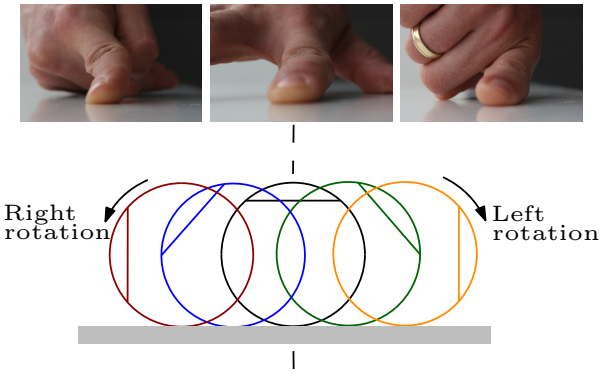

Figure 1: Illustration of the idea behind circular warping. The top row shows the rotation around the longitudinal axis which we want to simulate. The bottom row shows how this rotation looks in the circular model. The circular finger slice is rotated and rolled off onto a flat plane.

Circular warping: A cylinder c parameterized by radius r_c and height h_c is used to model the shape of the finger. For a given contactless fingerprint image I, we choose $r_c = \frac{w}{2}$ and $h_c = \frac{h}{2}$ where w denotes the width and h the height of the fingerprint image. We think of model warping as of a simulated roll-off motion around the longitudinal finger axis onto a flat "roll-off" plane L. An example of this process is illustrated in Figure 1. To find the point (L_x, L_y) on the roll-off plane L that corresponds to the point (I_x, I_y) in the fingerprint image I, we need to calculate the arc length of the circular curvature for each horizontal cylinder slice. The resulting warping function that solves this task is shown in Eqn. 1.

$$\begin{aligned} L_x &= r_c \cdot arcsin\left(\frac{I_x}{r_c}\right) \\ L_y &= I_y \end{aligned} \tag{1}$$

Elliptical warping: Alternatively, taking into account that each slice of the finger is shaped more like an ellipse rather than a circle, we can approximate the shape of the finger using an 3D ellipsoid e parameterized by the length of the major axis a_e, the length of the minor axis b_e and the height h_e. Similar to the authors in [13], we consider a fixed ratio of 1.2 between the major and minor axis where $b_e = \frac{a_e}{1.2}$. h_e is again chosen based on the height of the fingerprint I. Similar to the cylindrical model, we need to "unfold" the fingerprint by simulating a roll-off motion onto a 2D plane L. To accomplish this we also need to compute the arc length of ellipse of each slice of the ellipsoid. Therefore recall the standard parametric representation of an ellipse

which is shown in Eqn. 2 where x and y represent points on the ellipse.

$$\begin{aligned} x &= a \cdot cos(t) \\ y &= b \cdot sin(t) \\ \text{where} \\ t &= \big[0, 2\pi\big) \end{aligned} \tag{2}$$

To calculate the arc length between two points (x_1, y_1), (x_2, y_2) on the ellipse, we first have to calculate the corresponding angles t_1 and t_2 using the parametric equation. Knowing both angles we can calculate the arc length using Eqn. 3.

$$L(t_1, t_2) = \int_{t_1}^{t_2} \sqrt{b^2\ cos^2(t) + a^2\ sin^2(t)}\ dt \tag{3}$$

Next, to take into account that to simulate the fingerprint roll-off motion we only have to simulate the roll-off motion for a single half-circle, we fix the lower integration boundary $t_1 = 0$. The result is the warping function shown in Eqn. 4. Also note the term $\frac{L_{max}}{2}$ which ensures that the origin of the roll-off plane L is shifted to the center of the unwarped image.

$$\begin{aligned} L_x &= \frac{L_{max}}{2} - \int_0^{T_x} \sqrt{b_e^2\ cos^2(t) + a_e^2\ sin^2(t)}\ dt \\ L_y &= I_y \\ \text{where} \\ T_x &= arccos\Big(\frac{I_x}{a_e}\Big) \\ L_{max} &= L(0, \pi) \end{aligned} \tag{4}$$

Bidirectional warping:

So far, the cylindrical as well as the ellipsoidal model, only address finger deformations in the direction of the transversal axis. However, the tip of the fingertip is not only bent in transversal direction but also in longitudinal direction. To simulate a rotation around the transversal axis (besides to the rotation around the longitudinal axis) as shown in Fig. 2, we need to extend the 3D parametric in a way to it also models the curvature of the fingertip. To accomplish this we extend the cylindrical model by rounding off the top part of a cylinder to model the fingertip. Figure 3 shows the front view, top view and side view of the parametric model for the finger. Unfolding this 3D model requires us to not only simulate a rotation around the longitudinal axis but also around the tranversal axis for top part of the fingertip. Looking at Figure 3, we can derive the equations for the heights $h_{XY}(x)$, $h_{XZ}(x)$ and $h_{YZ}(y)$ for each point x or y on the x-axis or y-axis. The resulting equations are shown in Eqn. 5.

Figure 2: Example of the transversal finger rotation which we want to simulate with the bidirectional model

$$\begin{aligned} h_{XY}(x) &= r_{max} \cdot sin\left(arccos\Big(\frac{x}{r_{max}}\Big)\right) \\ h_{XZ}(x) &= r_{max} \cdot sin\left(arccos\Big(\frac{x}{r_{max}}\Big)\right) \\ h_{YZ}(y) &= r_{max} \cdot sin\left(arccos\Big(\frac{y}{r_{max}}\Big)\right) \end{aligned} \tag{5}$$

As can be seen in Eqn. 5, the height equation is the same for every view. Hence, the radius of the warping circle $r(\star)$ for any point $\star$ can be defined as shown in Eqn. 6.

$$r(\star) = h_{XY}(\star) = h_{XZ}(\star) = h_{YZ}(\star) \tag{6}$$

Combining Eqn. 6 with the warping equation of the cylindrical model (Eqn. 1) yields the warping equation for the bidirection warping model shown in Eqn. 7.

$$\begin{aligned} L_x &= \begin{cases} r(I_y) \cdot arcsin\Big(\frac{I_x}{r(I_y)}\Big) & \text{if } I_y \geq 0 \\ r_{max} \cdot arcsin\Big(\frac{I_x}{r_{max}}\Big) & \text{if } I_y < 0 \end{cases} \\ L_y &= \begin{cases} r(I_x) \cdot arcsin\Big(\frac{I_y}{r(I_x)}\Big) & \text{if } I_y \geq 0 \\ I_y & \text{if } I_y < 0 \end{cases} \end{aligned} \tag{7}$$

3. Experimental setup

To evaluate how the different warping models presented in Sec. 2 affect the contactless to contact-based comparison performance, we used a commercial state-of-the-art FP recognition system (Neurotechnology VeriFinger SDK 11.1) to extract FP templates from three different datasets and to compare them using the full match protocol. The full match protocol computes all possible permutations of contactless to contact-based FP pairs. We compute and report the comparison performance for three different datasets using the EER.

3.1. Datasets

In this work, three datasets consisting of 2D contactless and contact-based fingerprints were acquired from 28 volunteers. Contactless fingerprints for each dataset were extracted from videos showing an individual's hand from different perspectives. These videos were recorded with an iPhone 10 running a camera app that allows to fix the

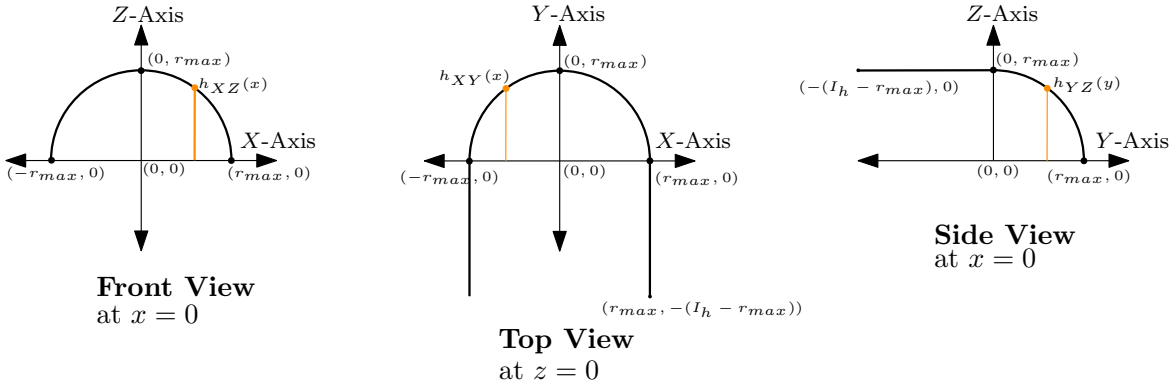

Figure 3: The finger model used for bidirectional warping shown in frontal, top and side view.

focal length of the camera lens. Fixing the focal length is beneficial as it allows to constraint the pixel density (Dots-per-Inch, a.k.a. DPI) of the contactless FPs. Since contact-based FPs are normalized to 500 DPI, the same needs to be done to contactless FPs. For obvious reasons, correcting the pixel density (DPI) is difficult if we do not know the resolution of the source image. However, due to the fixed lens setting, we can conclude that contactless FP images in our dataset which appear to be in-focus should exhibit a pixel density of around 900 DPI. To identify whether a contactless FP is in-focus or not, we first segmented and cropped out the fingertips from each video frame using a segmentation network (Deeplab [1]). We then assessed the quality of each fingerprint with the quality metric proposed in [8].

Dataset A (DB-A): The dataset is composed of 880 contactless FP images and 880 contact-based FP images captured from eleven individuals (eight fingers per individual). Fingertips of the index, middle, ring and pinky fingers were extracted from the video frames as explained above and ranked according to their quality. We then selected the ten highest quality frames available for each finger by hand. With "by hand" we mean that the correctness/quality of each image was verified by a human. For instance, images which exhibit a high quality score but are strongly rotated have not been added to the dataset. Contact-based samples were captured using the Greenbit DactyScan84C FP scanner. Ten contactless FPs of each finger were captured from each individual. Sample images from the dataset are shown in Figure 4a.

Dataset B (DB-B): The dataset is composed of 1360 contactless FP images and 680 contact-based FP images captured from 17 individuals (eight fingers per individual). Two videos (indoor/outdoor) were recorded from each hand of the individual. As in the case of DB-A, we selected the ten highest quality contactless FP images of each finger by hand. Five contact-based fingerprints of each finger were captured using a Suprema RealScan-G1 FP scanner. Sample images from the dataset are shown in Figure 4b.

Dataset C (DB-C): To increase the credibility of EERs for experiments where score fusion is applied, we decided to build another dataset with an increased number of genuine pairs out of *DB-B*'s raw video footage. The dataset uses the same videos and contact-based FPs as dataset *DB-B*. However, in contrast to *DB-B* we fully automatically extracted and selected the ten highest quality FP images for each finger in every single video. Consequently, the dataset has almost twice as many contactless FP images (2680 contactless images) as dataset *DB-B*. Note that by "fully automatic" we mean that contactless FP images extraction and selection entirely relies on the output of the segmentation network and quality metric — no human validating the data was involved. For this reason, we also expect *DB-C* to be more challenging than dataset *DB-B*. Sample images from the dataset are shown in Figure 4c.

3.2. FP image comparison pipeline

Given a contactless FP as well as a contact-based FP sample, we first applied one of the three warping models presented in Sec. 2 to the contactless RGB FP image. Examples of the warped images can be found in Fig. 5. We then postprocessed the unwarped FP using the FP enhancement technique which has been shown to work well for contactless images in [8]. Applying the enhancement technique to the contactless FP, the unwarped image is first transformed to the greyscale domain where grey value inversion as well as horizontal flipping is applied. Next, the image is de-blurred by substracting an average-filtered version of the image from the greyscaled and flipped imprint. In the last step, CLAHE [16] is used to enhance the contrast of the image followed by area adaption. Area adaption en-

(a) Dataset DB-A

(b) Dataset DB-B

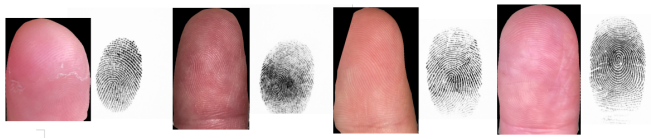

(c) Dataset DB-C

Figure 4: Contactless and contact-based FP samples from each of the three datasets

sures that the contactlessly captured FPs have similar shapes to contact-based samples.

After warping and enhancing of the contactless FP, the resulting FP is compared against the contact-based FP using a commercial state-of-the-art FP recognition system (Neurotechnology VeriFinger SDK 11.1). As we already pointed out, the pixel density (DPI) plays an important role when comparing FPs. To address the problem of varying FP template resolutions, VeriFinger SDK provides an option to specify the DPI of the given image. Note that if the option was not given, we would have to rescale the image to 500 DPI ourselves. As we know that contactless images in our dataset have approx. 900 DPI, we test three different types of DPI settings: *850 DPI*, *950 DPI* and *DPI Fused*. In the case of *DPI Fused*, the unwarped and enhanced FP is compared against the contact-based FP two times (using 850 DPI and 950 DPI). The higher score is then used as the final match score.

3.3. Multi-image FP comparison using score fusion

The fact that we have captured multiple contactless FP images of the same finger, raises the question whether we can somehow combine images of the same finger to the comparison performance. A naive strategy is max/mean score fusion. Given a set of contactless FP images (ten samples in our case) and a single contact-based FP image, we compare each contactless sample against the contact-based sample. Based on the chosen score fusion strategy, we either selected the maximum match score or mean match score for the selected samples. Note that we only report fusion results for datasets *DB-C* as score fusion has the drawback of reducing the number of genuine/imposter comparison scores and so the credibility of the measured EER. For example, in case of *DB-A* the initial number of genuine comparison scores (when no score fusion is applied) was 8800. Applying score fusion reduced to number to only 880. In case of *DB-B*, the number of genuine comparison scores was reduced from 6800 to 680. Hence, the resolution of the FMR axis is only 0.11% and 0.15%, respectively. In the case of *DB-C* we at least retain 1340 genuine comparison scores resulting in a FMR axis resolution of 0.07% when fusing the scores.

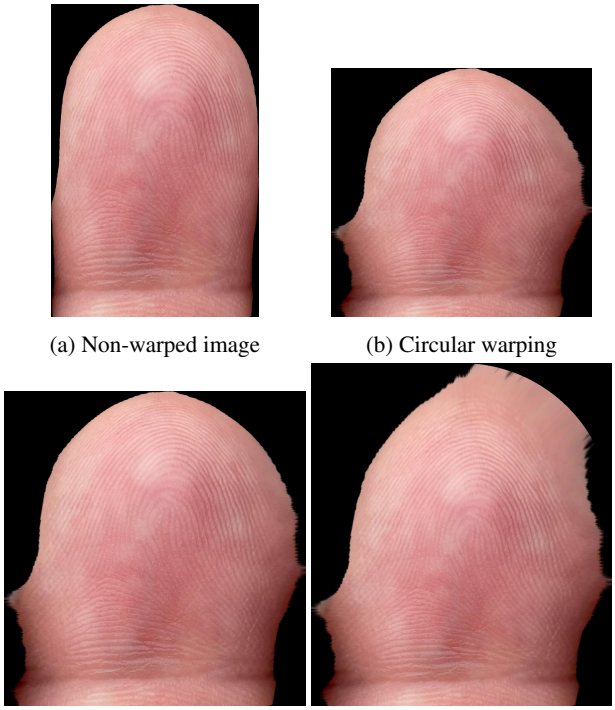

(a) Non-warped image (b) Circular warping

(c) Elliptic warping (d) Bidirectional warping

Figure 5: Comparison of different warping models applied to the non-warped image (top-left).

4. Experimental results

4.1. The impact of FP warping on the comparison performance

Table 1 shows the contactless to contact-based FP comparison performance (EER in %) for the different datasets and pixel densities. As can be seen in the results, the choice of the pixel density has a strong impact on the EER. Looking at the scenario where no warping is applied (warping model "None"), we can notice that EERs are considerably different depending on whether the pixel density is set to 850 DPI or 950 DPI. For instance, in the case of *DB-A*, the EER is only 1.62% for *850 DPI* but 3.47% for *950 DPI*. The

Warping model	DB-A			DB-B			DB-C		
	850 DPI	*950 DPI*	*DPI Fused*	*850 DPI*	*950 DPI*	*DPI Fused*	*850 DPI*	*950 DPI*	*DPI Fused*
None	1.62%	3.47%	1.79%	2.93%	2.38%	1.82%	2.48%	2.56%	1.83%
Circular	0.85%	1.95%	0.78%	3.42%	1.69%	1.31%	2.65%	1.85%	1.52%
Elliptical	0.88%	2.47%	0.93%	2.95%	1.77%	1.31%	2.49%	1.97%	1.53%
Bidirectional	0.84%	2.01%	0.88%	4.58%	1.62%	1.42%	3.81%	1.85%	1.66%

Table 1: Comparison of the contactless to contact-based FP comparison performance (EER in %) of the different warping models. The best (lowest) EER in each column is highlighted in green.

Warping model	No Score Fusion			Max Score Fusion			Mean Score Fusion		
	850 DPI	*950 DPI*	*DPI Fused*	*850 DPI*	*950 DPI*	*DPI Fused*	*850 DPI*	*950 DPI*	*DPI Fused*
None	2.48%	2.56%	1.83%	1.01%	1.09%	0.87%	1.13%	1.27%	0.97%
Circular	2.65%	1.85%	1.52%	1.10%	0.88%	0.96%	1.22%	0.81%	0.82%
Elliptical	2.49%	1.97%	1.53%	1.09%	1.09%	0.79%	1.05%	1.05%	0.74%
Bidirectional	3.81%	1.85%	1.66%	1.12%	0.81%	0.70%	1.94%	0.74%	0.75%

Table 2: Comparison of the contactless to contact-based FP comparison performance (EER in %) for dataset *DB-C* when max/mean score fusion is applied. The best (lowest) EER in each column is highlighted in green.

contrary is the case for *DB-B*. The EER has decreased from 2.93% (*850 DPI*) to 2.38% (*950 DPI*). Fortunately, score fusion of different DPIs seems to be a reasonable option to cope with the problem of different pixel densities. As can be seen in the columns *DPI Fused*, the reported EERs tend to be relatively robust.

Taking a look at the overall comparison performance, we can see that warping almost always provides better results than omitting the warping step. In particular it is interesting to see that the simplest warping method (Circular warping) worked best most of the time, especially in the case of *DPI Fused*. This suggest that it is not worth applying the more complex warping methods. Note that in the case of *DB-A* (*DPI Fused*), the EER decreased by more than half (from 1.79% to 0.78%). In the case of *DB-B* and *DB-C* the EER decreased by around 0.5% and 0.3% in the *DPI Fused* setting, respectively. However, it should also be mentioned that in some cases warping has increased the EER, i.e., in the case of *DB-B* (*850 DPI*) and *DB-C* (*850 DPI*). The fact that this behavior becomes apparent for all warping methods might be caused by the choice of the pixel density.

4.2. Computational costs

To be able to use a warping method in practice, not only the comparison performance but also the time required to warp an image play an important role. Hence we want to briefly comment on the computational costs of each method. Circular warping was straightforward to implement and the fastest warping method in our experiment with an average warping time of 4.4 ms/image. Elliptical warping was more challenging to implement in a time-efficient manner. Unfortunately, there exists no closed form solution for the integral which has to be solved to obtain the arc length of an ellipse and solving the integral numerically is slow. In our experiment, elliptical warping using a numeric integral solver took 652 ms/image. However, we were able to achieve a significant speed by precomputing points located on the unit ellipse. For a given image, we then rescaled the precomputed point set and linearly sampled the relevant points. This way it took only 5.7 ms to elliptically warp an image. The slowest method in our expirement was the bidirectional warping. Unfortunately, computing the inverse mapping of the bidirectional warping function is difficult as it requires to solve a complex non-linear equation system. For this reason bidirectional warping of an image took around 13 sec/image using our implementation. However, we strongly believe that it is possible to speed up the bidirectional warping by means of a rescaling/sampling approach.

4.3. The impact of score fusion on the comparison performance

As discussed in Sec. 3.3 the availability of multiple contactless images raises the question whether fusing the match scores for those image can be used to improve the FP comparison performance. The results for dataset *DB-C* when max/mean score fusion is applied are shown in Table 2. As can be immediately seen in the table, score fusion clearly improves the comparison performance no matter if warping

is applied or not. In both fusion methods, max and mean fusion, improve the EER by more than a half. The best results are achieved if max/mean score fusion is combined with DPI fusion. This seems obvious since this is more or less a combination of best of both worlds.

Again we can notice a similar behavior as reported in Table 1 where warping improves the comparison performance in almost any case. However, this time circular warping can not be claimed to work best. Instead, taking into account that elliptical warping is on a par with bidirectional warping in the *Mean Fusion* case, we can claim bidirectional warping to work best. Why this is the case is not entirely clear at this point. Further experiments using more data need to be done to investigate this phenomenon.

Finally, we briefly want to comment on the score fusion results for *DB-A* and *DB-B*. As explained in Sec. 3.3 the fusion score analysis for these datasets lack credibility due to the limited number of genuine comparison scores wherefore we decided to not provide a detailed comparison of the different warping methods when score fusion is applied. However, we can still comment on the overall trend. Similar to *DB-C*, we could see max/mean score fusion clearly improves the result. For pixel density, in case of max fusion *DB-A* / *DPI Fused* / *No warping* the EER dropped from 1.79% to 0.26% and in case of *DB-B* / *DPI Fused* / *No warping* it dropped from 1.82% to 0.37%. Considering the limited number of genuine comparison scores, we can only say that warping overall tends to improve the result.

5. Conclusion

In this work, we have dealt with the problem of physical deformations in the context of 2D contactless to 2D contact-based FP comparison. We have proposed and investigated three simple parametric warping models (circular, elliptical and bidirectional warping) which can warp a contactless FP to better match contact-based FPs. Besides that, we have shown score fusion to be an effective and easy way to improve the FP comparison performance for scenarios where multiple contactless FP images for the same finger are available. All methods were tested on a dataset composed of challenging contactless FP images which were captured with a standard smartphone and strong perspective distortions. Our results show that warping, in particular circular warping, is an simple tool to improve the contactless to contact-based FP comparison performance. Using circular warping we were able to decrease the EER from 1.79% to 0.78% and 1.82% to 1.31% on our datasets, respectively.

References

[1] L.-C. Chen, Y. Zhu, G. Papandreou, F. Schroff, and H. Adam. Encoder-decoder with atrous separable convolution for semantic image segmentation. In *ECCV*, 2018.

[2] Y. Chen, G. Parziale, E. Diaz-Santana, and A. K. Jain. 3d touchless fingerprints: Compatibility with legacy rolled images. In *2006 Biometrics Symposium: Special Session on Research at the Biometric Consortium Conference*, pages 1–6. IEEE, 2006.

[3] A. Dabouei, S. Soleymani, J. Dawson, and N. M. Nasrabadi. Deep contactless fingerprint unwarping. In *2019 International Conference on Biometrics (ICB)*, pages 1–8. IEEE, 2019.

[4] J. J. Engelsma, K. Cao, and A. K. Jain. Learning a fixed-length fingerprint representation. *IEEE Transactions on Pattern Analysis and Machine Intelligence*, 2019.

[5] L. Ericson, S. Shine, I. ManTech Advanced Systems International, and U. S. of America. Evaluation of contactless versus contact fingerprint data phase 2 (version 1.1). *DOJ Office Justice Programs, I. ManTech Adv. Syst. Int., Fairmont, WV, USA, Tech. Rep*, 249552, 2015.

[6] S. A. Grosz, J. J. Engelsma, and A. K. Jain. C2cl: Contact to contactless fingerprint matching. *arXiv preprint arXiv:2104.02811*, 2021.

[7] F. Karegar, J. S. Pettersson, and S. Fischer-Hübner. Fingerprint recognition on mobile devices: Widely deployed, rarely understood. In *Proceedings of the 13th International Conference on Availability, Reliability and Security*, pages 1–9, 2018.

[8] C. Kauba, D. Söllinger, S. Kirchgasser, A. Weissenfeld, G. Fernández Domínguez, B. Strobl, and A. Uhl. Towards using police officers business smartphones for contactless fingerprint acquisition and enabling fingerprint comparison against contact-based datasets. *Sensors*, 21(7):2248, 2021.

[9] J. Libert, J. Libert, J. Grantham, B. Bandini, K. Ko, S. Orandi, and C. Watson. *Interoperability assessment 2019: Contactless-to-contact fingerprint capture*. US Department of Commerce, National Institute of Standards and Technology, 2020.

[10] C. Lin and A. Kumar. Matching contactless and contact-based conventional fingerprint images for biometrics identification. *IEEE Transactions on Image Processing*, 27(4):2008–2021, 2018.

[11] A. Ross and R. Nadgir. A calibration model for fingerprint sensor interoperability. In *Biometric Technology for Human Identification III*, volume 6202, page 62020B. International Society for Optics and Photonics, 2006.

[12] A. Ross and R. Nadgir. A thin-plate spline calibration model for fingerprint sensor interoperability. *IEEE Transactions on Knowledge and Data Engineering*, 20(8):1097–1110, 2008.

[13] H. Tan and A. Kumar. Towards more accurate contactless fingerprint minutiae extraction and pose-invariant matching. *IEEE Transactions on Information Forensics and Security*, 15:3924–3937, 2020.

[14] S. Wood and C. Wilson. Studies of plain-to-rolled fingerprint matching using the nist algorithmic test bed (atb), 2004-09-27 2004.

[15] W. Zhou, J. Hu, S. Wang, I. Petersen, and M. Bennamoun. Performance evaluation of large 3d fingerprint databases. *Electronics letters*, 50(15):1060–1061, 2014.

[16] K. Zuiderveld. Contrast limited adaptive histogram equalization. *Graphics gems*, pages 474–485, 1994.